Article:
Nar, K., Majewski, C. orcid.org/0000-0003-3324-3511 and Lewis, R. orcid.org/0000-0002-4300-0540 (2022) A comprehensive characterisation of Laser Sintered Polyamide-12 surfaces. Polymer Testing, 106. 107450. ISSN 0142-9418

https://doi.org/10.1016/j.polymertesting.2021.107450

Polymer Testing 106 (2022) 107450

Contents lists available at ScienceDirect

Polymer Testing

journal homepage: www.elsevier.com/locate/polytest

A comprehensive characterisation of Laser Sintered Polyamide-12 surfaces

Kieran Nar *, Candice Majewski, Roger Lewis

Department of Mechanical Engineering, University of Sheffield, Sheffield, UK

ARTICLE INFO

Keywords:
Additive Manufacturing
Laser Sintering
Polyamide-12
Surface characterisation
Sub-surface microstructure

ABSTRACT

Polymer Laser Sintering (LS) is a powder-based Additive Manufacturing (AM) process known for its ability to produce highly complex geometries. The powder-based nature of the process means it intrinsically produces components with characteristic surface topographies abundant with features, as well as relatively high surface roughnesses, when compared with traditional polymer processing techniques such as Injection Moulding. There are a number of factors which influence the resultant surface topography of LS components and consequently affect their functional performance, particularly when subject to dynamic contact. However, little work has been carried out to date to fully understand these surface determining mechanisms. The scope of this research was to comprehensively characterise the surface topography of LS PA12 specimens and to specifically understand how resultant roughness is a function of applied energy density; XY location across the powder bed; part surface orientation; measurement technique and roughness descriptor. Results showed that the roughness profiles of top and bottom surfaces of cube-shaped samples were distinct in both size and shape. Top surfaces had positive Skewness values and were therefore dominated by asperity peaks, whereas bottom surfaces were neither entirely featureful of peaks nor valleys. Moreover, micro-CT analysis provided insight into how the sub-surface microstructure was affected by part orientation and applied energy density. Resultant binary images revealed the upward-facing section of a cylindrical LS PA12 specimen orientated 45° with respect to the powder bed to be less dense than the downward-facing section of the same sample. This work provides a benchmark for future Polymer Powder Bed Fusion (PBF) studies, specifically when characterising the friction and wear properties of resultant samples.

1. Introduction

Today, Additive Manufacturing is well established within industry, where its adoption continues to grow [1,2]. A plethora of layer-wise AM techniques exist, and a variety of materials can be processed, including ceramics, metals, polymers and composites [3,4].

Polymer Laser Sintering is a Powder Bed Fusion processing technique that has become increasingly widely adopted due to its ability to build functional end-use components without the requirement for support structures [5]. While LS can be used to process a variety of polymers, this work will focus on Polyamide-12 (also referred to as Nylon-12) as it is the most well-established polymer for Laser Sintering [6] due to its wide processing window [7] and relatively good recyclability [8]. In addition, some resultant tensile properties of LS PA12 parts, notably stiffness and tensile strength are comparable with those obtained via Injection Moulding [6,9].

Despite extensive research having already been carried out to characterise the mechanical properties of LS PA12 components, an incomplete understanding of part quality continues to hinder the further adoption of LS within industry [2,10,11]. Therefore, additional research is still required to thoroughly understand the functional performance of LS PA12 components. Given the importance of surface finish in many end-use applications, particularly when LS polymer components are subject to dynamic contact, and the limited literature available, this work will focus on comprehensively characterising the resultant topographies of LS PA12 surfaces.

1.1. Characterisation of LS surfaces

1.1.1. Roughness parameters

Laser Sintered surfaces are primarily characterised through roughness, either 2- or 3-dimensionally. Gadelmawla et al. [12] produced an exhaustive catalogue of parameters that describe surface roughness. Details of several widely-adopted roughness parameters are given in

* Corresponding author.
E-mail address: knar1@sheffield.ac.uk (K. Nar).

https://doi.org/10.1016/j.polymertesting.2021.107450
Received 1 October 2021; Received in revised form 19 November 2021; Accepted 10 December 2021
Available online 11 December 2021

Table 1
Descriptions of the roughness parameters used within this study.

Surface Roughness Parameter	Abbreviation	Description	Mathematical Definition
Arithmetic Mean Height	S_a	The average of the distribution of surface heights per unit sampling area.	$S_a = \frac{1}{A}\int\int_A \lvert Z(x,y)\rvert \, dxdy$
Root Mean Square (RMS)	S_q	The standard deviation of the distribution of surface heights [12] per unit sampling area.	$S_q = \sqrt{\frac{1}{A}\int\int_A \{Z(x,y)\}^2 \, dxdy}$
Maximum Peak-to-Valley Height	S_z	The sum of the maximum peak height and maximum valley depth within the surface area evaluated.	$S_z = maxZ - \lvert minZ\rvert$
Skewness	S_{sk}	Describes whether the distribution of bulk material within a surface profile is above or below the mean plane. If a profile has a negative Skewness value, valleys are a more dominant feature than peaks within a profile, and vice versa.	$S_{sk} = \frac{1}{S_q^3}\frac{1}{A}\int\int_A Z^3(x,y) \, dxdy$
Kurtosis	S_{ku}	Describes the sharpness of a surface height distribution [18]. Profiles with $S_{ku} > 3$, are leptokurtic and have relatively many points of major maxima and minima. Whereas platykurtic distributions ($S_{ku} < 3$) have relatively fewer points of major maxima and minima per sampling area [12].	$S_{ku} = \frac{1}{S_q^4}\frac{1}{A}\int\int_A Z^4(x,y) \, dxdy$

Table 1.

Amplitude parameters describe how a surface profile changes in the vertical direction and are most frequently used to characterise surface topographies. They can also be sub-categorised as to whether they primarily describe the size or shape of surface peaks and valleys. The most frequently observed size descriptors in polymer LS literature are the Arithmetic Mean Height [13–17], Root Mean Square (RMS) [14] and Maximum Peak-to-Valley Height [13,14,16] parameters.

Amplitude probability density functions are used to describe shape, specifically the symmetry and sharpness of a surface profile through Skewness and Kurtosis, respectively, as can be seen in Fig. 1.

Furthermore, amplitude probability density functions can differentiate between surface profiles that are different in shape, but have the same resultant Arithmetic Mean Height [12]. For non-Gaussian profiles, such as LS PA12 surfaces, roughness shape descriptors may therefore be equally, or even potentially more, useful than size descriptors for correlating surface topography with functional performance.

At present, and to the best of the author's knowledge, the use of amplitude probability density functions to comprehensively characterise polymer Laser Sintered surfaces has yet to be observed within literature.

1.1.2. Characterisation methods

Numerous techniques for characterising AM surfaces have been reported in the literature. The most common roughness determining method is Contact Profilometry (CP) [13,14,16,19–22]. However, more recently, alternative areal surface metrology techniques have gained popularity. These include: Focus Variation (FV) [16,23–25] Confocal Microscopy (CM) [16,26], GelSight [13,27] and X-Ray Computed Tomography (XCT) [28,29]. These techniques are mostly non-contact and quick to execute with vertical resolutions within the nanometer range [30,31]. Launhardt et al. [16] compared Arithmetic Mean and Maximum Peak-to-Valley Height results obtained using Contact Profilometry and optical measurement methods when characterising LS PA12 surfaces. They found the optical results measured by Focus Variation were the most similar in terms of trend with the results collected by Contact Profilometry.

1.2. Factors affecting LS surfaces

Many factors intrinsically affect the resultant surface roughness of Laser Sintered PA12 components. These factors can largely be categorised as powder properties [32,33], processing parameters [34,35] and/or surface orientation effects.

1.2.1. Powder properties

Schmid et al. [36] demonstrated the sensitivity between powder production technique, resultant particle morphology, sintered part properties and surface quality. More specifically, particle size, shape [37] and size distribution all impact a powder's ability to flow [33]. Powders should have good flowability to allow for the consistent deposition of both thin and homogeneous layers [38]. Additionally, it is common practice to reuse powders to improve the economic feasibility of LS. The quantities in which recycled and virgin material are present within a powder is known as its refresh ratio. It is well established that refresh ratios of $\geq$ 50% virgin material should be employed when good surface quality, free from the 'orange peel' effect, is required [39–41].

1.2.2. Processing parameters

With regards to processing parameters, Sachdeva et al. [14], Mavoori et al. [42] and Bacchewar et al. [43] all used optimisation design of experiment methodologies to identify which processing parameters had

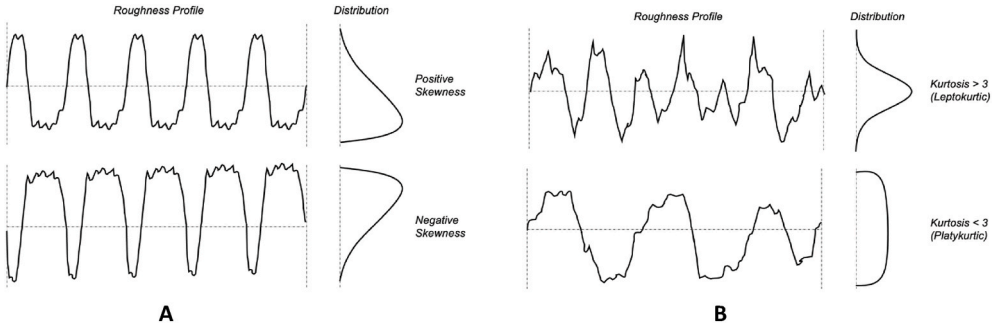

Fig. 1. Example profiles with extreme (A) Skewness and (B) Kurtosis distributions.

the greatest effect on the resultant roughness of LS Polyamide surfaces. They found laser power, bed temperature and build orientation to be the most influential processing parameters, respectively. Despite the differences, it is clear that these factors should be considered in any study in this area.

1.2.3. Surface orientation

Part orientation is user-defined and directly influences the resultant roughness of LS surfaces. More specifically, Schmidt et al. [36] and De Pastre et al. [29] observed that top and bottom surfaces built parallel to the powder bed had smaller resultant S_a and S_q values than side surfaces of the same samples.

Furthermore, Schmidt et al. [36] also identified top surfaces to have greater resultant S_a and S_q values than bottom surfaces despite them having the same surface orientation with respect to the powder bed. Also, Zhu et al. [44] and Triantaphyllou [45] both demonstrated that Skewness could be used to distinguish between upward- and downward-facing surfaces built by High Speed Sintering (HSS) and Selective Laser Melting (SLM), respectively.

Surfaces orientated non-parallel to the powder bed will contain layer-wise discontinuities intrinsic to the Laser Sintering build process. This 'stair-stepping' effect [43] is a function of both processing parameters and powder properties, and exacerbated by re-entrant features, such as partially sintered powder particles. Both Launhardt et al. [16] and Zhu et al. [44] prescribed that surfaces that contain re-entrant or undercut features cannot accurately be characterised by Contact Profilometry and optical line-of-sight surface metrology techniques.

Table 2
Processing parameters used.

Processing parameters	Value
Laser power (W)	18, 21 and 24
Beam spacing (mm)	0.25
Scan speed (mm/s)	2500
Bed temperature (°C)	170
Layer thickness (mm)	0.1
Build volume dimensions (XYZ) (mm × mm × mm)	170 × 220 × 290

With the exception of amplitude probability density functions, prior efforts have been made to isolate the aforementioned variables that influence the surface topographies of LS PA12 components. However, these resultant surfaces are intrinsically sensitive and thus a complex function of both process and evaluation. Therefore, this work aimed to comprehensively characterise the surfaces of Laser Sintered PA12 specimens in a single study and thus systematically elucidate both processing parameters and evaluation methods with resultant roughness size and shape descriptors.

More specifically, resultant surface roughness and sub-surface microstructure were characterised as a function of applied energy density; XY location across the powder bed; part surface orientation; measurement technique; roughness descriptor; and percentage porosity.

2. Material and methods

2.1. Material

Polyamide-12, specifically PA2200 supplied by EOS GmbH, was used, as it is the most well-documented polymer for LS. A refresh ratio of 50% virgin and 50% once-used material, mixed by rotary tumbling for approximately 20 minutes, was chosen to best emulate conventional practice. All samples were produced from the same batch of powder.

2.2. Specimens

An EOS Formiga P100 system, programmed with the processing parameters listed in Table 2, was used to perform the Laser Sintering process. Different laser powers (18 W, 21 W and 24 W) were selected to vary the magnitude of applied energy density to each tier of the build to 28.8 $mJmm^{-2}$, 33.6 $mJmm^{-2}$ and 38.4 $mJmm^{-2}$, respectively. No contour scan was included. These resultant energy density values were calculated using Eq. (1) below,

$$\text{Energy Density} = \frac{\text{Laser Power}}{\text{Beam Spacing} \times \text{Scan Speed}} \quad (1)$$

The build layout can be seen in Fig. 2, different specimen geometries

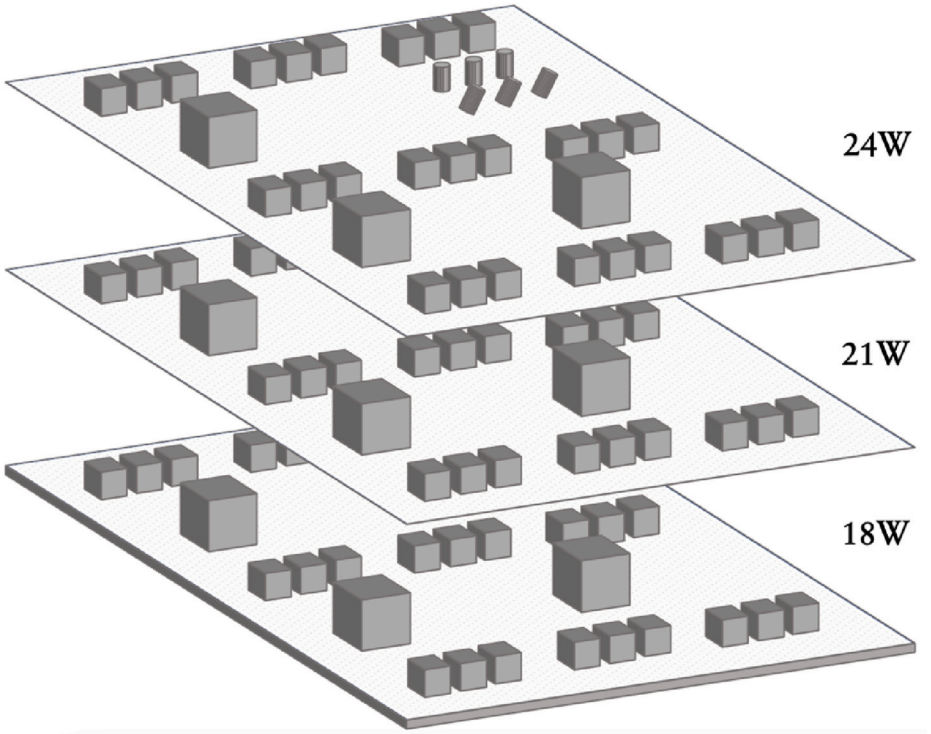

Fig. 2. Laser Sintering build layout.

were designed depending on the respective analysis they were intended for. More specifically, 16 × 16 × 16mm cube-shaped specimens were produced for Contact Profilometry; 8 × 8 × 8mm cube-shaped specimens were produced for Focus Variation; and 5 × 6mm (DxL) cylindrical-shaped specimens were produced for micro-CT.

Once Laser Sintered, compressed air was used to remove loose powder particles from each surface of each specimen. Efforts were made to ensure this process was repeated consistently.

2.3. Methods

Specimens were characterised using metrology techniques of increasing geometrical dimensional capability, from 2-dimensional profile to 3-dimensional areal and volume-based analysis methods. This was to better understand how the size of evaluation region effects the accuracy in characterising the true non-Gaussian topographies of LS PA12 surfaces.

2.3.1. Characterisation

2.3.1.1. Roughness parameters

. This investigation evaluated the size and shape of roughness profiles using the descriptors: S_q, S_z, S_{sk}, S_{ku} and equivalent R-parameters. Detailed descriptions of all these parameters are given in Table 1. In this investigation RMS roughness was selected as the primary parameter for describing the size of measured surface profiles. Statistically, S_q is more sensitive to large deviations from the mean line than S_a [12], so is more capable of characterising asperity tip detail.

2.3.1.2. Contact profilometry

. Contact profilometry was performed using a Mitutoyo Surftest SJ-400 to measure 2-dimensional surface profiles and compute their R-roughness parameters. Measurements were recorded over an evaluation length of 4 mm at a transverse speed of 0.5 mm s^{-1}, using a stylus with tip radius and angle of 2 μm and 60°, respectively. Gaussian filtering with a cut-off length of 0.8 mm was applied.

2.3.1.3. Focus Variation microscopy

. Areal surface roughness was measured by Focus Variation (FV) microscopy, specifically using an Alicona InfiniteFocusSL system. During FV, a vertical array of images was captured, where the distance between each image was equal to the vertical resolution of the scan. To extract depth information, each pixel within each image was compared with neighbouring pixels to gain a measure of local contrast [23]. The size of the region selected to evaluate local contrast is better known as lateral resolution. The determined relative contrast of each pixel was then compared with the relative contrast of each pixel with the same X and Y coordinates throughout the vertical image array. Finally, the Z-location of each pixel with the greatest relative contrast with respect to the length of the vertical image array was used to compute the Z-coordinate of the scanned surface. A typical areal FV scan of a LS PA12 surface is shown in Fig. 3.

In this investigation a ×5AV objective lens was used with a vertical resolution of 550 nm and the smallest lateral resolution required to generate a complete scan. The specimen surfaces were illuminated with a coaxial polarised ring light before a 3.7 × 3.7 mm area was scanned. Surface roughness information was then obtained from each scan using an evaluation area of 2.5 × 2.5 mm without any applied filtering.

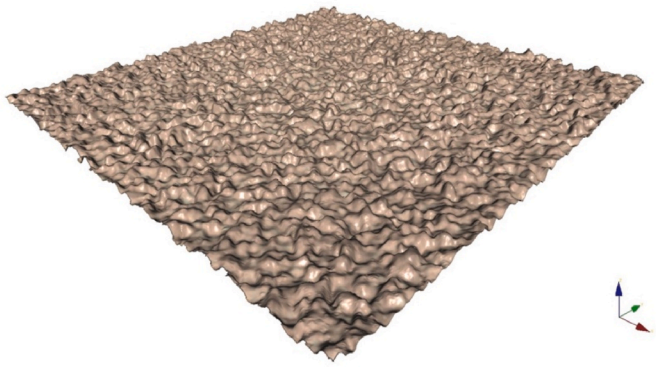

Fig. 3. A typical FV scan.

2.3.1.4. Micro-CT

. Small scale XCT, more commonly referred to as micro-CT, was utilised to better understand the relationship between part orientation, applied energy density, surface roughness and sub-surface microstructure.

Sub-surface microstructure is a term frequently used within literature, particularly within the context of polymer tribology [15,46,47], however to the best of the authors' knowledge no explicit definition for sub-surface depth currently exists. In this investigation the sub-surface region of interest was chosen to include material within a depth of between 4 and 5 times the measured S_z of the surface, as well as the surface itself, of the sample cross-section being examined. This corresponded to a depth of 1 mm from the asperity peaks of each sample.

A Skyscan 1172 was used to scan the cylindrical specimens. This was achieved using an accelerating voltage of 40 kV; 148 μA source current; 295 ms exposure time; reconstructed voxel size (or image pixel size) of 4.18 μm; 180° rotation with a step size of 0.7° and no filtering. In total 4 specimens were scanned, 3 vertically orientated parts each built using different laser powers (18 W, 21 W and 24 W), as well as a 21 W part built at 45° with respect to the powder bed.

Post-scanning, NRecon and CTAn was used for reconstruction and to generate binary images, respectively.

3. Results

3.1. Profile analysis

Figs. 4–7 provide a comparison between the resultant roughness of the top and bottom surfaces of specimens built at 18 W, 21 W and 24 W and evaluated by Contact Profilometry. For each applied laser power 3 different specimens were evaluated.

As shown in Fig. 4, there was a distinct difference between the resultant R_q of top and bottom surfaces. More specifically, top surfaces had greater R_q roughness magnitudes than bottom surfaces from the same samples. This relationship between part surface orientation and resultant R_q was independent of applied laser power, as shown in Table 3.

However, the variability in results obtained by Contact Profilometry were relatively large, as indicated by range bar lengths in Fig. 4 and computed mean range values presented in Table 3. Moreover, no distinct relationship between the variability in results, applied laser power or

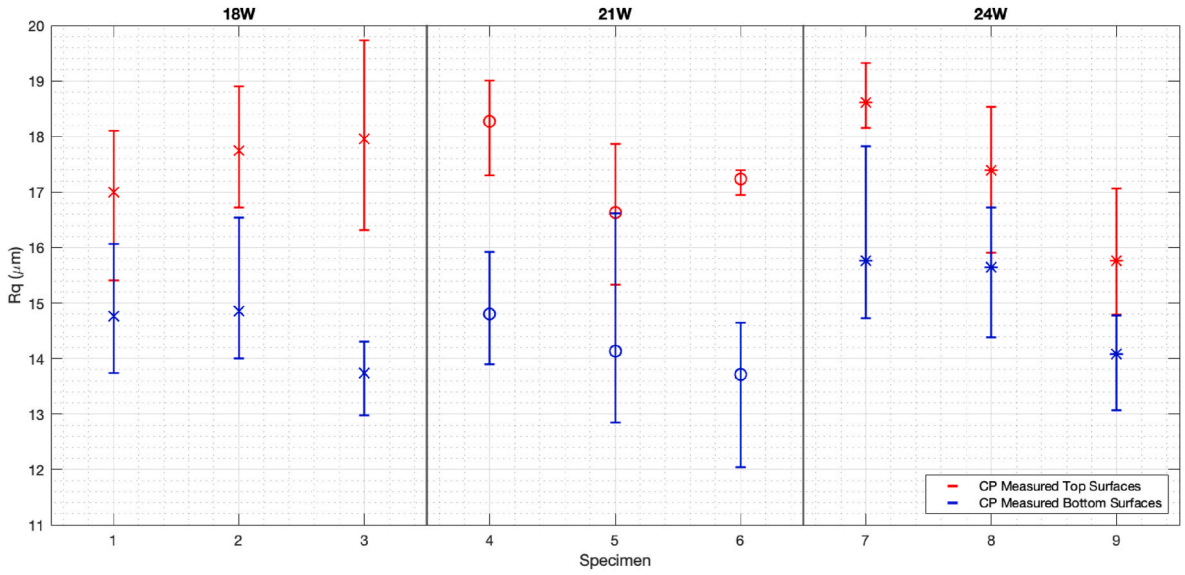

Fig. 4. A comparison of R_q results collected by Contact Profilometry of top and bottom surfaces of specimens built at different applied energy densities.

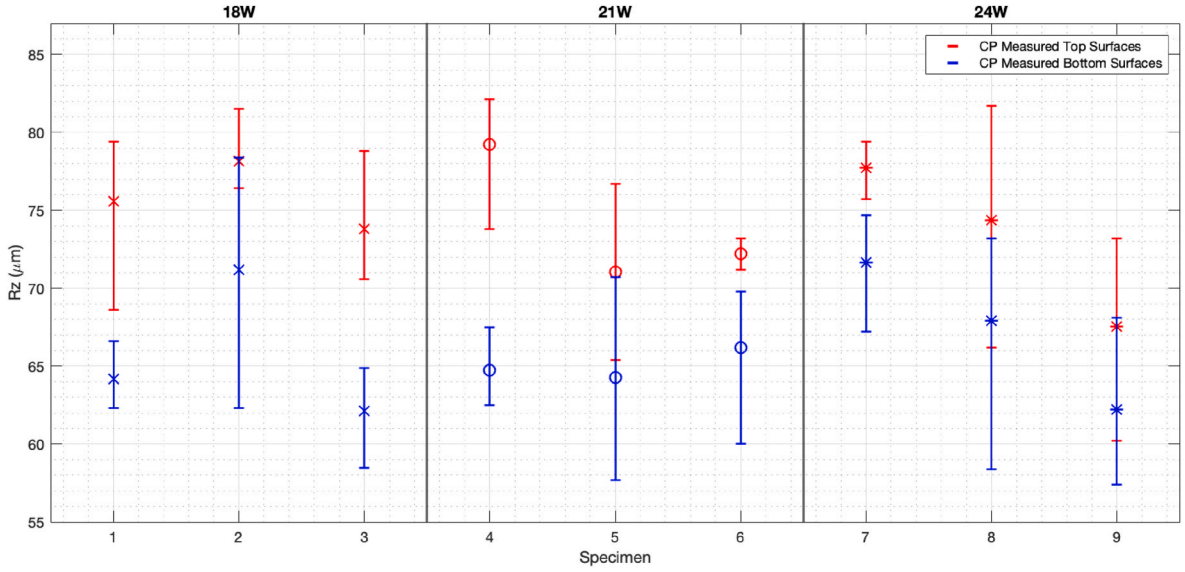

Fig. 5. A comparison of R_z results collected by Contact Profilometry of top and bottom surfaces of specimens built at different applied energy densities.

part surface orientation could be determined.

Resultant Maximum Peak-to-Valley Height, R_z, results are shown in Fig. 5, again a distinct difference in the size of top and bottom surface roughness profiles was observed. Similar to Fig. 4, top surfaces had greater resultant roughness magnitudes than bottom surfaces of the same samples.

Furthermore, R_z is analytically sensitive to anomalous peaks and valleys, so significant variability, as represented by range bar length, was intrinsically expected.

Distinction in profile shape, specifically symmetry as characterised by Skewness, of top and bottom surfaces was not observed in Fig. 6. Independent of part surface orientation, resultant R_{sk} values centred

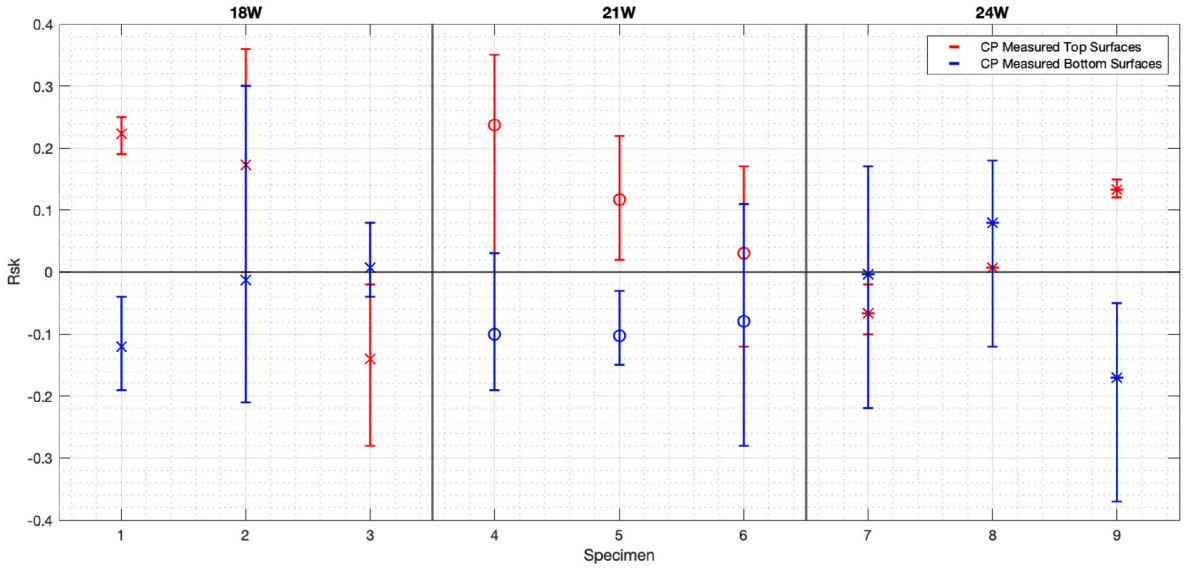

Fig. 6. A comparison of R_{sk} results collected by Contact Profilometry of top and bottom surfaces of specimens built at different applied energy densities.

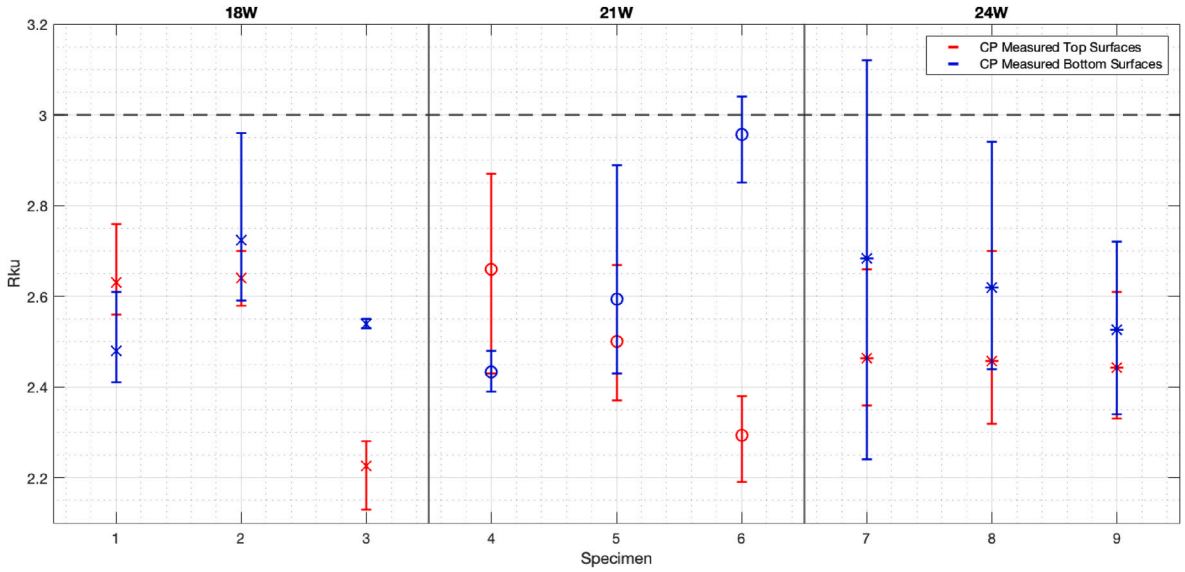

Fig. 7. A comparison of R_{ku} results collected by Contact Profilometry of top and bottom surfaces of specimens built at different applied energy densities.

Table 3
Overall mean resultant S_q and corresponding range values of top and bottom surfaces of specimens built at 18W, 21W and 24W and evaluated by Contact Profilometry.

	18 W		21 W		24 W	
	Mean S_q (μm)	Mean range value (μm)	Mean S_q (μm)	Mean range value (μm)	Mean S_q (μm)	Mean range value (μm)
Top	17.57	2.76	17.38	1.56	17.25	2.02
Bottom	14.45	2.06	14.22	2.80	15.16	2.38

around zero, which suggested LS PA12 surfaces were Gaussian with symmetrical topographies, relative to the mean planes of these surfaces.

Fig. 7 shows the resultant Kurtosis results of specimen surfaces measured using Contact Profilometry as a function of part surface orientation and applied laser power. Resultant mean R_{ku} results were all less than the critical value of 3, which suggested that all top and bottom surfaces were dominantly platykurtic and thus relatively non-spiky.

The lack of definition in profile shape, as measured by Contact Profilometry and characterised by both Skewness and Kurtosis, is discussed in greater detail in **Section 4.2**.

3.2. Areal analysis

Areal analysis of LS PA12 surfaces by Focus Variation also augmented understanding of how resultant roughness varied across the powder bed. The layout of Figs. 8–11 are partly illustrative with respect to the exact positioning of parts across the powder bed, and therefore not perfectly to scale.

Variation in surface roughness, specifically S_q, across the powder bed can be seen in Fig. 8, where maximum and minimum values from each individual surface data set have also been included to highlight the variability of Focus Variation within this study.

For both top and bottom surfaces, it can be seen in Fig. 8 that S_q remained relatively constant, independent of applied energy density and location across the powder bed. More specifically, the mean S_q values of

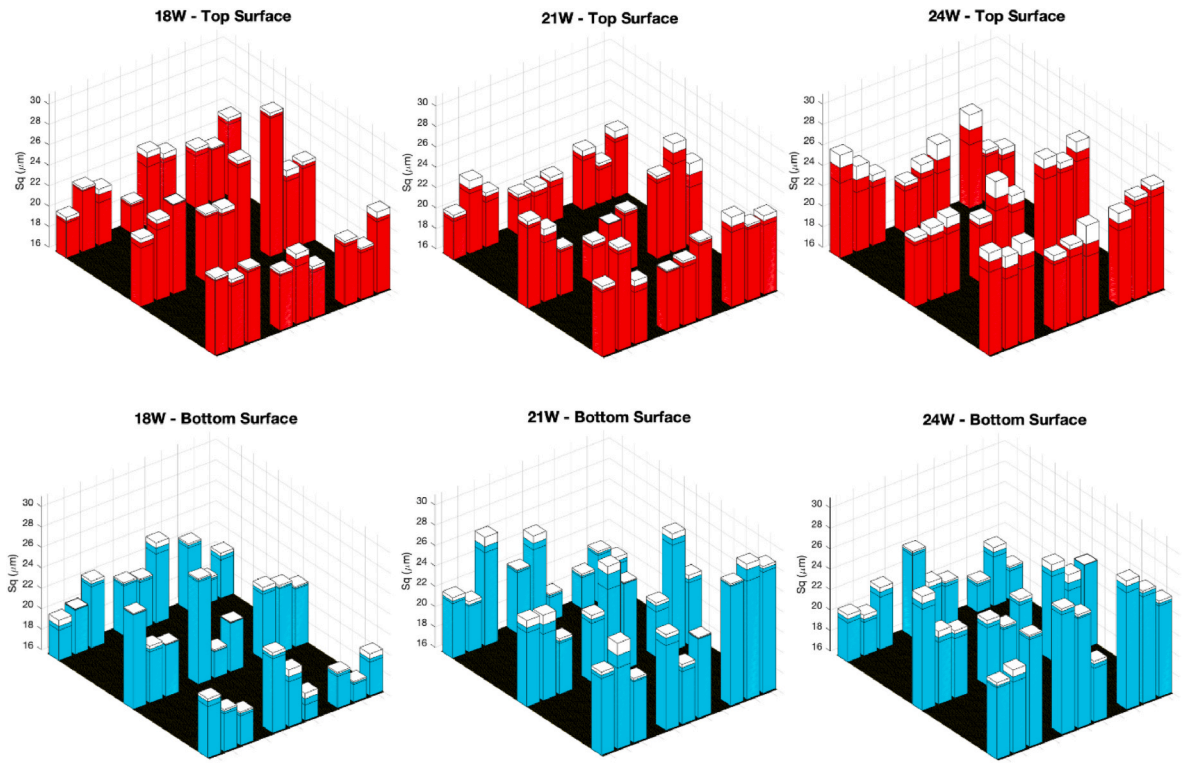

Fig. 8. A comparison of mean S_q results (including range bars) of top and bottom surfaces measured by Focus Variation of specimens built across the powder bed with different applied energy densities.

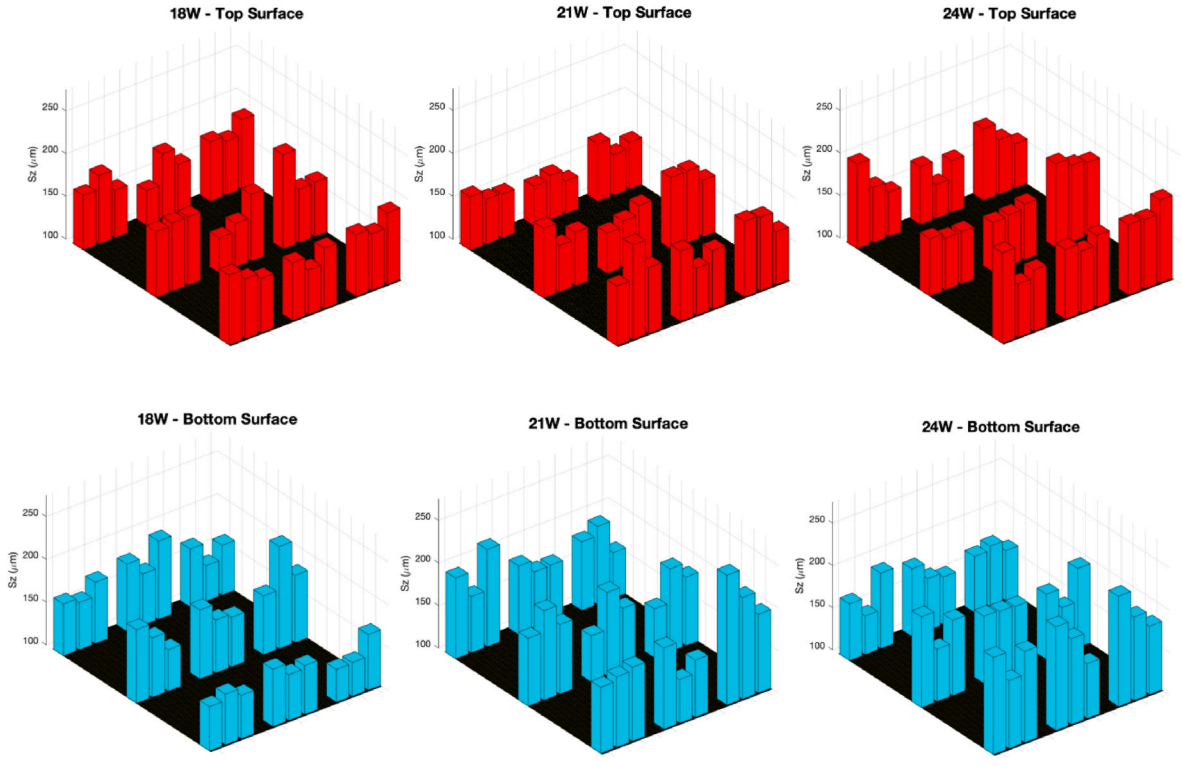

Fig. 9. A comparison of mean S_z results collected using FV of top and bottom surfaces of specimens built across the powder bed with different applied energy densities.

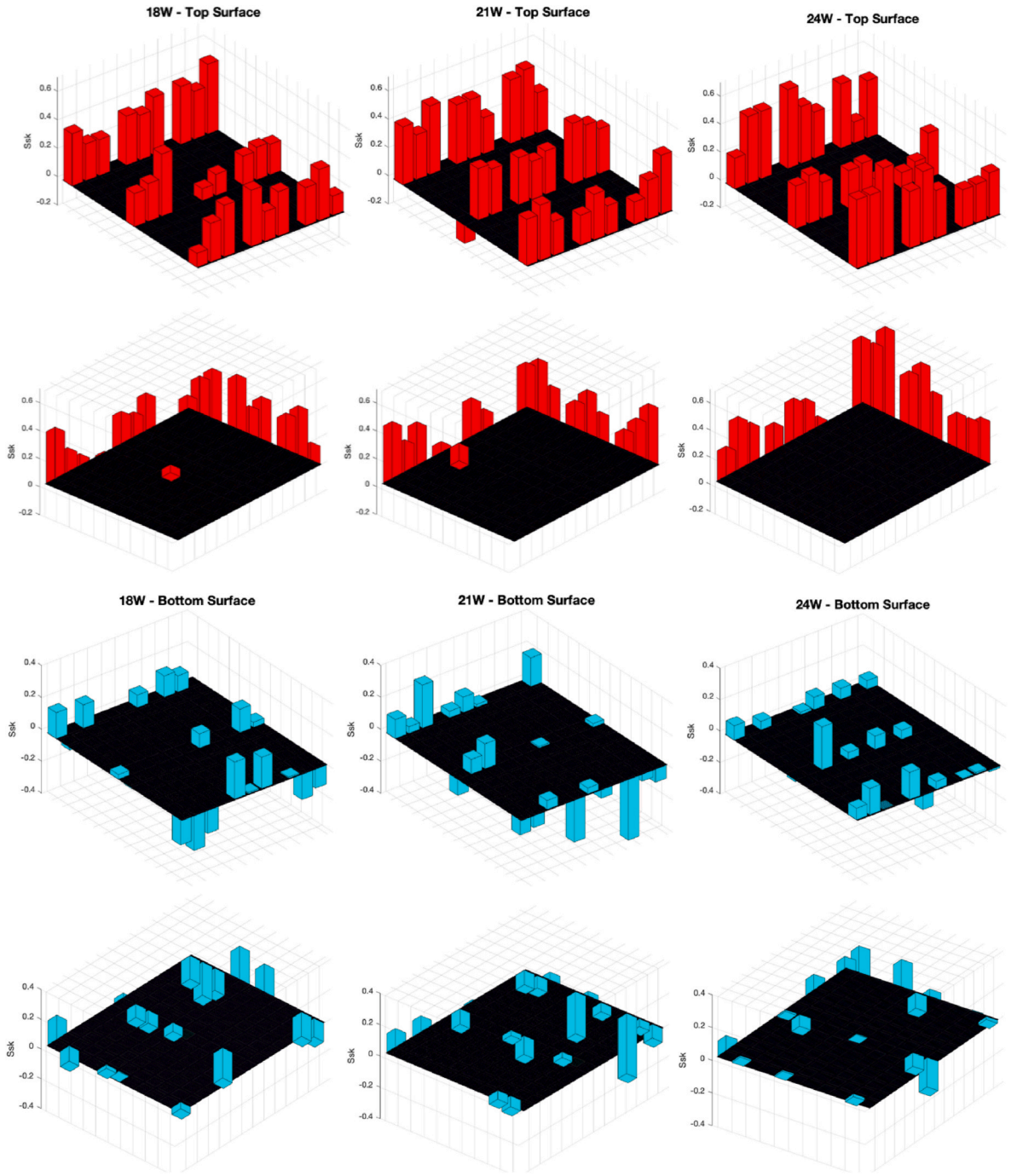

Fig. 10. A comparison of mean S_{sk} results collected using FV of top and bottom surfaces of specimens built across the powder bed with different applied energy densities.

top surfaces built at laser powers of 18 W, 21 W and 24 W were 22.61 μm, 22.07 μm and 23.16 μm, respectively. Similarly, the mean S_q values for bottom surfaces were 21.06 μm, 23.35 μm and 23.13 μm, respectively.

The difference between maximum and minimum bar heights for each surface is equivalent to range bar length. Top surface variability increased with laser power, mean differences between maximum and minimum bar heights for all top surfaces built at 18 W, 21 W and 24 W were 0.66 μm, 0.85 μm and 1.68 μm, respectively. However, this correlation was not observed for bottom surfaces of the same samples.

As shown in Fig. 9, no significant variation in Maximum Peak-to-Valley Height roughness, independent of applied laser power, across the powder bed was observed.

When analysing the shape of LS PA12 surfaces it can be seen in Fig. 10 that the Skewness values of top surfaces were almost all positive (p-value = 0.025). Comparing this with a significance level of $\alpha = 0.05$, it can be asserted with statistical confidence that the top surfaces of the LS PA12 components analysed had a positive Skewness. Therefore, these top surfaces were peak dominated because the bulk of the material that made up these surfaces existed mostly below each respective mean plane.

Furthermore, increasing the applied laser power from 18 W to 21 W and 24 W also increased the resultant top surface mean Skewness of each tier of samples from 0.273 to 0.321 and 0.352, respectively.

However, bottom surfaces of the same samples had resultant Skewness values that were neither entirely positive nor negative, as can be seen in Fig. 10. No correlation was observed between Skewness, location or applied energy density. This is discussed in greater detail in **Section 4.1**.

In the samples analysed and presented in Fig. 11, no statistically significant correlation (p-value $> \alpha$) between Kurtosis with location, part surface orientation or applied laser power was seen. An opaque reference plane at the critical Kurtosis value of 3 was also included in Fig. 11 to highlight the lack of distinction.

3.3. Volume analysis

Fig. 12 includes binary images of cross-sections of cylindrical samples analysed using micro-CT to highlight how the sub-surface microstructures of LS PA12 components are affected by applied laser power and part orientation. The cross-sections presented are from the middle of each specimen in its longest direction, though percentage porosity results were mean values computed from 4 cross-sections evenly distributed throughout each specimen's resultant scan volume.

Resultant percentage porosities of the vertically built samples at applied laser powers of 18 W, 21 W and 24 W were 32.02%, 24.56% and 28.24%, respectively.

Also, a specimen built at 21 W, but orientated at 45° with respect to the powder bed was scanned, intrinsically this allowed both upward- and downward-facing surface and sub-surface sections to be analysed. This can be observed in the binary cross-sectional image labelled 21 W 045° in Fig. 12, where a distinction between the upward- and downward-facing sections of the specimen can be clearly seen. The downward-facing section of the 21 W 045° sample had a significantly smoother surface with less sub-surface porosity than the upward-facing section of the same sample. More specifically, using personal judgement to divide the 21 W 045° sample binary image into two distinct sections allowed each to be further analysed, this divide can be seen in Fig. 13. Resultant percentage porosities of the upward- and downward-facing sections were computed to be 32.79% and 21.81%, respectively.

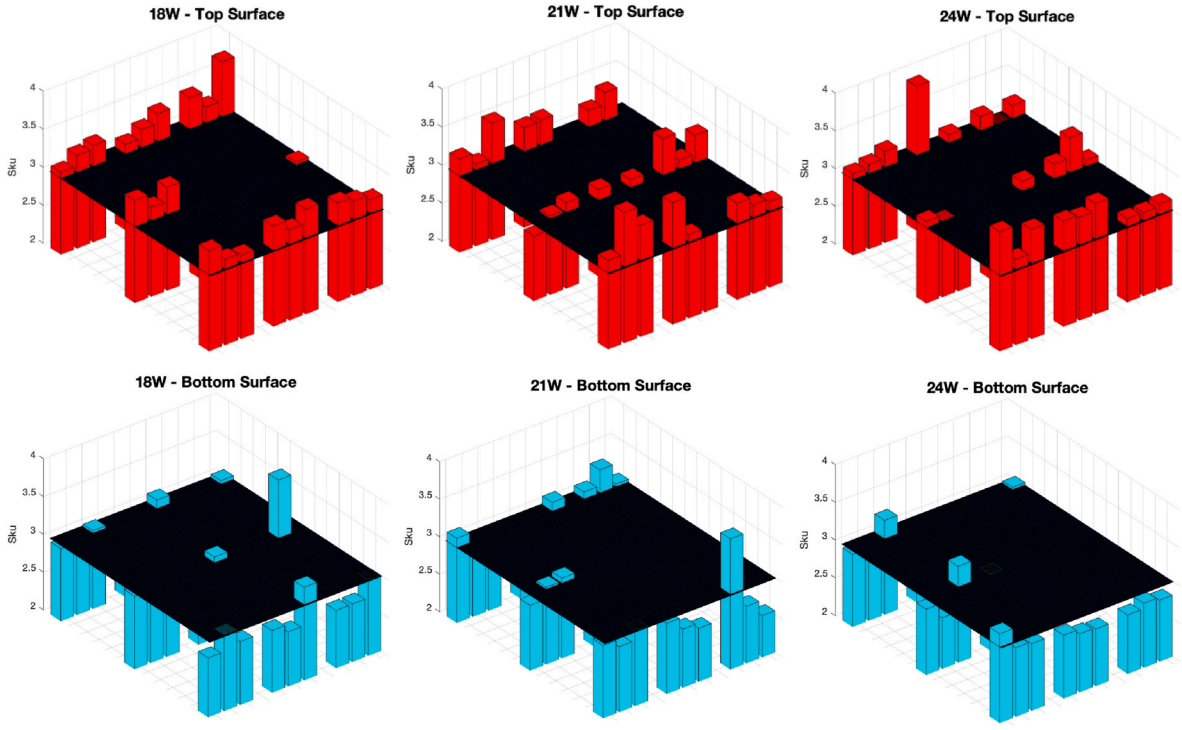

Fig. 11. A comparison of mean S_{ku} results collected using FV of top and bottom surfaces of specimens built across the powder bed with different applied energy densities.

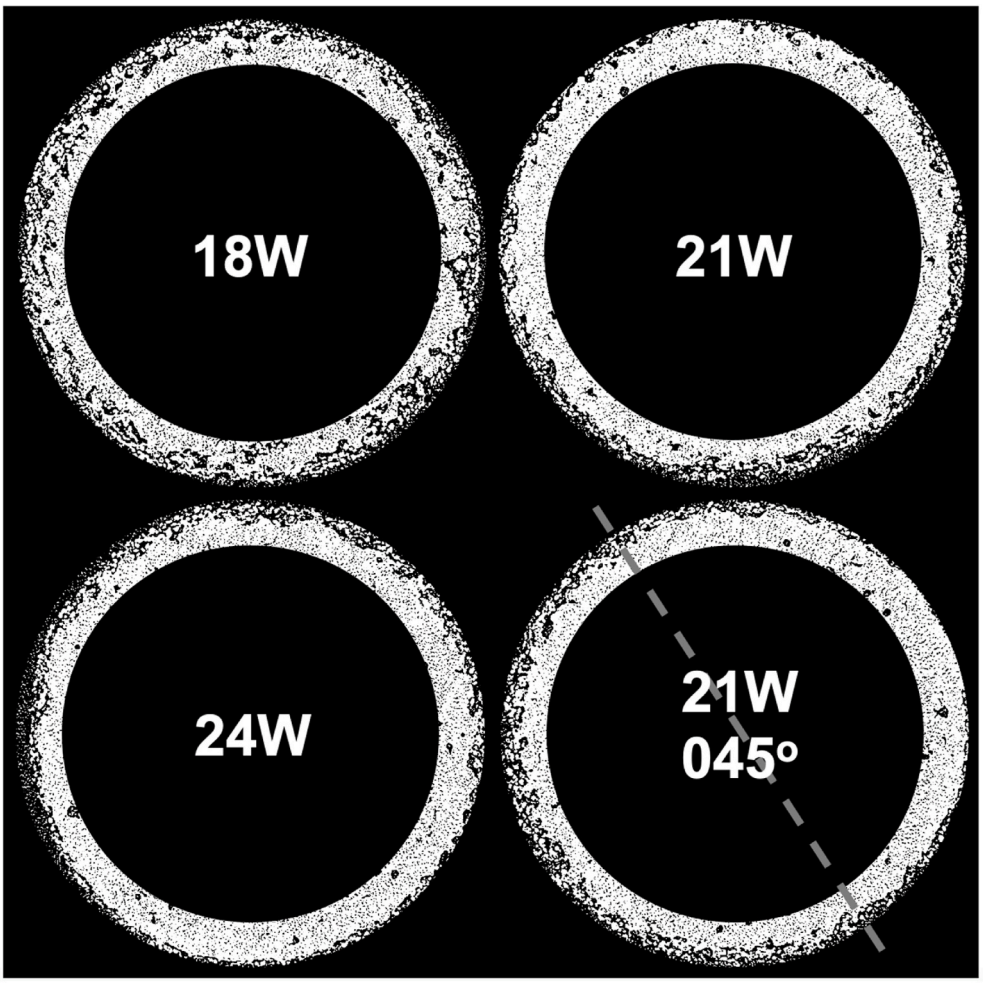

Fig. 12. Binarised Micro-CT images of specimens built with different applied energy densities and orientations.

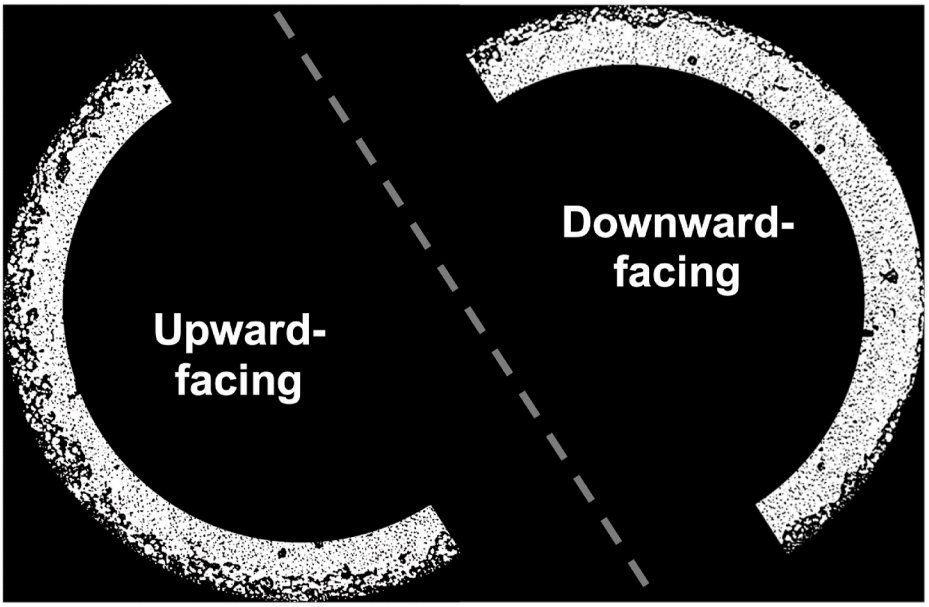

Fig. 13. Divided and binarised sections of the 21 W 045° sample.

4. Discussion

4.1. Resultant LS PA12 surfaces

As shown in Section 3.2, the lack of variation in surface roughness, including both size and shape parameters, across the powder bed promotes the suitability of using LS (specifically the EOS Formiga P100) to produce parts in greater quantities within individual builds, whilst guaranteeing consistent surface topographies on comparable surfaces. More specifically, no specific regions of the powder bed were identified as locations which resulted in parts with significantly higher or lower S_q roughness values.

However, mean R_q results obtained using Contact Profilometry did show top surfaces to have greater resultant magnitudes than bottom surfaces of the same samples, an observation shared by Schmidt et al. [36]. Therefore, part surface orientation should be considered when Laser Sintering functional PA12 components.

Maximum Peak-to-Valley Height roughness data presented in Figs. 5 and 9 was in good agreement with Contact Profilometry and Focus Variation results collected by Laundhart et al. [16] who also measured the R_z and S_z of LS PA12 samples. However, LS PA12 surfaces are abundant with defects [48] therefore Maximum Peak-to-Valley Height descriptors, which intrinsically are determined by the single most defective feature present within a surface, cannot accurately characterise entire profiles or areas.

When comparing the shape of top and bottom surface profiles measured by Focus Variation and described by Skewness an apparent difference was observed. Top surfaces had dominantly positive Skewness values, whereas the S_{sk} of bottom surfaces were neither entirely positive nor negative. Work by De Pastre et al. [29] also asserts that top surfaces of LS PA12 specimens are peak dominated when evaluated by Focus Variation, but also when measured by Coherence Scanning Interferometry and XCT after the application of both S- and L-filtering. A potential explanation as to why top surfaces have positive resultant Skewness values could be explained through the mechanism of powder particle adhesion. Upon the top layer being sintered, powder particles in the following pass of material could adhere to the former top surface. So, the adhesion between the original top surface and powder particles in the subsequent layer forms the new top surface of the component. This is best illustrated in Fig. 14, where the grey and orange profiles represent the original and new top surfaces, respectively.

Furthermore, this mechanism of top surface modification through exterior powder particle adhesion should theoretically be affected by applied energy density which determines the magnitude of residual heat energy in the original top surface, as well as the thickness of the subsequent powder layer. The former was observed within this study, in Section 3.2 increasing laser power also increased the magnitude of the resultant mean positive Skewness. The latter, layer thickness, was observed by Bacchewar et al. [43] to be the most influential processing parameter (excluding part surface orientation) to affect the roughness of upward-facing surfaces. More specifically, greater layer thicknesses should increase the height of asperity peaks as well as the volume of bulk material below the mean plane of the top surface and therefore the positivity of resultant Skewness values. Furthermore, in Section 3.2 it was demonstrated that increasing applied energy density also increased the variability in repeat readings obtained by Focus Variation. Theoretically, increasing applied energy density should promote the mechanism of powder particle adhesion and thus the number of surface irregularities within a topography. Consequently, evaluating these surface topographies becomes more difficult and variability in resultant roughness data is expected to increase.

This hypothesised mechanism of top surface powder particle adhesion has been investigated further in unpublished work, where a distinct difference in resultant top surface Skewness was observed in specimens built with and without additional finish layers. More specifically, LS PA12 specimens built without additional finish layers were found to have negative resultant top surface Skewness values and were therefore valley dominated. Whereas top surfaces built with additional finish layers were again found to have positive resultant Skewness values.

Unlike top surfaces, the layer of powder beneath the original bottom surface is still subject to applied energy during the initial layers of the build. This exposure to heat energy could result in the partial coalescence, rather than adhesion, of exterior powder particles with the original bottom surface. This mechanism of partial coalescence of exterior powder particles should therefore have a less distinct effect on the resultant Skewness of a surface when compared with the mechanism of adhesion. The magnitude of applied energy density and layer thickness should therefore determine how much heat the exterior powder particles beneath the original bottom surface are exposed to. Again work by Bacchewar et al. [43] supports this hypothesis, when analysing downward-facing surfaces they found laser power, as well as layer thickness and build orientation, to be the significant parameters influencing R_a.

For both Contact Profilometry and Focus Variation, no discernible link between Kurtosis roughness results, applied energy density and part surface orientation could be established. This means that either the sharpness of resultant LS PA12 surfaces are entirely random, or surface metrology techniques of greater sophistication than those used in this study are required to characterise Kurtosis.

4.2. Difference in areal and profile results

Analysing range bar magnitudes in Figs. 4 and 8 allowed the variability of Contact Profilometry and Focus Variation surface metrology methods to be compared. R_q results obtained by Contact Profilometry had greater variability than 3-dimensional RMS results obtained using Focus Variation. This suggests that areal measurements are more appropriate than 2-dimensional profiles when computing roughness

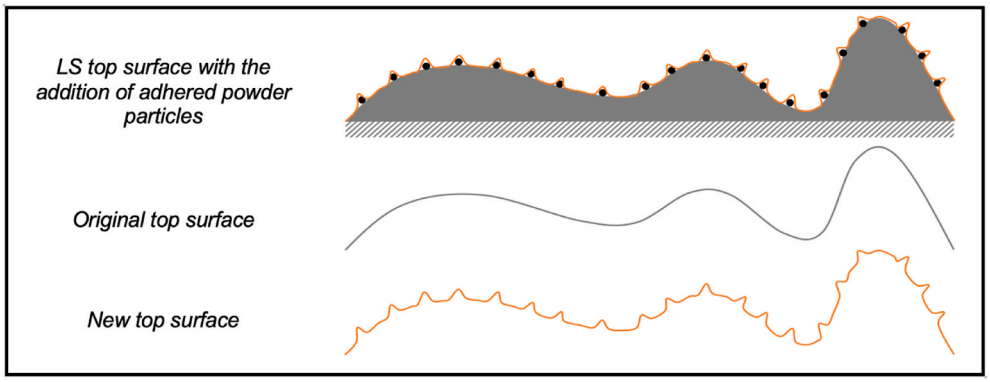

Fig. 14. An illustration representing the proposed mechanism of top surface modification through exterior powder particle adhesion.

results because evaluation areas better represent the total surface area of the component being examined.

The difference in measured profile and areal roughness size results was significant, with resultant S_z values being approximately double that of equivalent profile magnitudes. A complete understanding as to why such a contrast in roughness size magnitudes measured by Contact Profilometry and Focus Variation occurs is still unclear. De Pastre et al. [29] suggested that optical effects when measuring translucent samples and asperity peak removal through scratching could both serve as possible explanations.

The 'Smoothing Effect' intrinsic to Contact Profilometry should also be considered. The finite geometry of the stylus tip results in micro-valley volume not being captured, as well as the over-evaluation of micro-peak volume. As a result, the volume distribution of the surface shifts away from the bulk of the specimen and towards the asperity tips. Consequently, a peak dominated surface profile with a positive Skewness could be incorrectly characterised by Contact Profilometry as having a symmetrical material distribution ($S_{sk} \sim 0$). This may help to explain why top surface Skewness results in Fig. 6 obtained using Contact Profilometry were centred around zero. In addition, tip angle as well as tip radius should be considered when interpreting results collected using Contact Profilometry. In this investigation the stylus tip had a radius of 2 μm and a tip angle of 60°, which meant that the tip size effectively doubled to a radius of 4 μm at only a distance of 4.6 μm from the tip point itself.

4.3. Resultant part sub-surface microstructures

The effectiveness of using micro-CT to characterise sub-surface microstructure was highlighted in Figs. 12 and 13.

Also, computing percentage porosities confirmed what was seen visually in Fig. 12, where the primary porosity inducing mechanisms transitioned from incomplete consolidation to excessive partial sintering of exterior powder as applied laser power increased. These mechanisms were apparent in the samples built vertically at applied laser powers of 18 W and 24 W, respectively. Whereas the specimen constructed at 21 W was subject to a synergistic balance of both mechanisms, thus why it had the lowest resultant percentage porosity.

Furthermore, after analysing the upward- and downward-facing sections of the 21 W 045° specimen in Fig. 13, it can be asserted that sub-surface microstructure, as characterised by percentage porosity, is a function of both applied energy density and part orientation. Visual analysis of Fig. 13 also suggested the surface roughness in terms of size of upward-facing surface sections to be larger than downward-facing surface sections. This supplements the Contact Profilometry results presented in **Section 3.1**. Further work should be carried out to explicitly correlate the surface roughness of LS PA12 components with sub-surface microstructure, specifically percentage porosity.

5. Conclusions

In this investigation, Contact Profilometry, Focus Variation and micro-CT were used to better understand how LS PA12 surfaces and sub-surfaces are a function of applied energy density; XY location across the powder bed; part surface orientation; measurement technique; roughness descriptor; and percentage porosity.

It was shown that the resultant roughness profiles of top and bottom surfaces of LS PA12 components are distinct in both size and shape. Top surface roughness profiles were dominated by asperity peaks and greater in amplitude than bottom surfaces, which were neither entirely featureful of peaks nor valleys. Therefore, when describing the topography of LS surfaces both size and shape descriptors should be used, for PA12 S_q and S_{sk} were determined to be the most appropriate. Furthermore, build location across the powder bed, had no observable effect on resultant part roughness parameters. In addition, micro-CT highlighted part orientation also significantly effects resultant sub-surface microstructure. Binarised scan imagery confirmed upward-facing sections had greater amplitude roughness's and porosity than downward-facing sections.

For the first time amplitude probability density functions were used to characterise Laser Sintered PA12 surfaces to describe the symmetry and shape of their resultant topographies. Now an insight into LS surface Skewness is known, surface orientation could be selected to optimise resultant part functional performance. More specifically, an understanding of whether a surface will be peak or valley dominated could correlate with the probability of microcrack initiation and thus forecast the onset of surface fatigue, and why particular friction and other wear mechanisms occur when these surfaces are subject to dynamic contact.

This research serves as foundational work and will be referred to, as well as advanced, when comprehensively characterising the functional performance of LS polymer components in future studies.

Funding

The authors would like to acknowledge the support of EPSRC (DTP account EP/N509735/1) for partially funding the PhD studentship this research is based on.

Author contributions

Kieran Nar: Conceptualization, Methodology, Formal analysis, Investigation, Writing - Original Draft, Visualization.

Dr Candice Majewski: Resources, Supervision, Project administration, Funding acquisition.

Professor Roger Lewis: Resources, Supervision, Project administration, Funding acquisition.

Declaration of competing interest

The authors declare the following financial interests/personal relationships which may be considered as potential competing interests: Kieran Nar reports financial support was provided by Engineering and Physical Sciences Research Council.

Acknowledgements

The author would like to thank Wendy Birtwistle for her assistance in preparing and executing the Laser Sintering build, and Dr Enrico Dall'ara for their advice and training when performing Micro-CT analysis.

References

[1] T. Wohlers, I. Campbell, O. Diegel, R. Huff, J. Kowen, Wohler Report 2019: 3D Printing and Additive Manufacturing, State of the Industry, Wohlers Associates, Fort Collins, 2019.
[2] Ernst & Young Global Limited, 3D Printing: Hype or Game Changer? - A Global EY Report 2019, 2019.
[3] S. Yuan, F. Shen, C.K. Chua, K. Zhou, Polymeric composites for powder-based additive manufacturing: materials and applications, Prog. Polym. Sci. 91 (2019) 141–168, https://doi.org/10.1016/j.progpolymsci.2018.11.001.
[4] H. Zarringhalam, N. Hopkinson, N.F. Kamperman, J.J. de Vlieger, Effects of processing on microstructure and properties of SLS Nylon 12, Mater. Sci. Eng. 435–436 (2006) 172–180, https://doi.org/10.1016/j.msea.2006.07.084.
[5] R.D. Goodridge, C.J. Tuck, R.J.M. Hague, Laser sintering of polyamides and other polymers, Prog. Mater. Sci. 57 (2012) 229–267, https://doi.org/10.1016/j.pmatsci.2011.04.001.
[6] Y. Wang, Z. Xu, D. Wu, J. Bai, Current status and prospects of polymer powder 3D printing technologies, Materials 13 (2020), https://doi.org/10.3390/ma13102406.
[7] M. Heinz Scholten, Haltern Wolfgang Christoph, Use of a nylon-12 for selective laser sintering 6 (281 B1) (2001) 245.
[8] B. Yao, Z. Li, F. Zhu, Effect of powder recycling on anisotropic tensile properties of selective laser sintered PA2200 polyamide, Eur. Polym. J. 141 (2020) 110093, https://doi.org/10.1016/j.eurpolymj.2020.110093.
[9] B. Van Hooreweder, D. Moens, R. Boonen, J.P. Kruth, P. Sas, On the difference in material structure and fatigue properties of nylon specimens produced by injection molding and selective laser sintering, Polym. Test. 32 (2013) 972–981, https://doi.org/10.1016/j.polymertesting.2013.04.014.
[10] Sculpteo, The State of 3D Printing 2020, 2020.

[11] Stratasys, Looking Forward : Additive Manufacturing in 2020. A Report from 3D Printing Users, 2020.
[12] E.S. Gadelmawla, M.M. Koura, T.M.A. Maksoud, I.M. Elewa, H.H. Soliman, Roughness parameters, J. Mater. Process. Technol. 123 (2002) 133–145, https://doi.org/10.1016/S0924-0136(02)00060-2.
[13] M. Vetterli, M. Schmid, K. Wegener, Comprehensive Investigation of Surface Characterization Methods for Laser Sintered Parts, 2018.
[14] A. Sachdeva, S. Singh, V.S. Sharma, Investigating surface roughness of parts produced by SLS process, Int. J. Adv. Manuf. Technol. 64 (2013) 1505–1516, https://doi.org/10.1007/s00170-012-4118-z.
[15] J. Guo, J. Bai, K. Liu, J. Wei, Surface quality improvement of selective laser sintered polyamide 12 by precision grinding and magnetic field-assisted finishing, Mater. Des. 138 (2017) 39–45, https://doi.org/10.1016/j.matdes.2017.10.048.
[16] M. Launhardt, A. Wörz, A. Loderer, T. Laumer, D. Drummer, T. Hausotte, M. Schmidt, Detecting surface roughness on SLS parts with various measuring techniques, Polym. Test. 53 (2016) 217–226, https://doi.org/10.1016/j.polymertesting.2016.05.022.
[17] S. Petzold, J. Klett, A. Schauer, T.A. Osswald, Surface roughness of polyamide 12 parts manufactured using selective laser sintering, Polym. Test. 80 (2019) 106094, https://doi.org/10.1016/j.polymertesting.2019.106094.
[18] F. Blateyron, The areal field parameters, in: R. Leach (Ed.), Characterisation Areal Surf. Texture, Springer Berlin Heidelberg, Berlin, Heidelberg, 2013, pp. 15–43, https://doi.org/10.1007/978-3-642-36458-7_2.
[19] R. Brown, C.T. Morgan, C.E. Majewski, Not just nylon… improving the range of materials for high speed sintering, Solid Free, in: Fabr. 2018 Proc. 29th Annu. Int. Solid Free. Fabr. Symp. - an Addit. Manuf. Conf. SFF 2018, 2020, pp. 1487–1498.
[20] F. Dangnan, C. Espejo, T. Liskiewicz, M. Gester, A. Neville, Friction and wear of additive manufactured polymers in dry contact, J. Manuf. Process. 59 (2020) 238–247, https://doi.org/10.1016/j.jmapro.2020.09.051.
[21] M. Vetterli, M. Schmid, W. Knapp, K. Wegener, New horizons in selective laser sintering surface roughness characterization, Surf. Topogr. Metrol. Prop. 5 (2017), 045007, https://doi.org/10.1088/2051-672x/aa88ee.
[22] A. Townsend, N. Senin, L. Blunt, R.K. Leach, J.S. Taylor, Surface texture metrology for metal additive manufacturing: a review, Precis. Eng. 46 (2016) 34–47, https://doi.org/10.1016/j.precisioneng.2016.06.001.
[23] L. Newton, N. Senin, C. Gomez, R. Danzl, F. Helmli, L. Blunt, R. Leach, Areal topography measurement of metal additive surfaces using focus variation microscopy, Addit. Manuf. 25 (2019) 365–389, https://doi.org/10.1016/j.addma.2018.11.013.
[24] J. Bai, S. Yuan, W. Chow, C.K. Chua, K. Zhou, J. Wei, Effect of surface orientation on the tribological properties of laser sintered polyamide 12, Polym. Test. 48 (2015) 111–114, https://doi.org/10.1016/j.polymertesting.2015.09.017.
[25] R. Leach, N. Senin, Focus Variation Measurement and Prediction of Surface Texture Parameters Using Machine Learning in Laser Powder Bed Fusion, vol. 142, 2020, pp. 1–12, https://doi.org/10.1115/1.4045415.
[26] A. Wörz, D. Drummer, Tribological anisotropy of selective laser sintered PA12 parts, Polym. Test. 70 (2018) 117–126, https://doi.org/10.1016/j.polymertesting.2018.06.028.
[27] L. Pagani, A. Townsend, W. Zeng, S. Lou, L. Blunt, X.Q. Jiang, P.J. Scott, Towards a new definition of areal surface texture parameters on freeform surface: Re-entrant features and functional parameters, Meas. J. Int. Meas. Confed. 141 (2019) 442–459, https://doi.org/10.1016/j.measurement.2019.04.027.
[28] F. Zanini, L. Pagani, E. Savio, S. Carmignato, Characterisation of additively manufactured metal surfaces by means of X-ray computed tomography and generalised surface texture parameters, CIRP Ann 68 (2019) 515–518, https://doi.org/10.1016/j.cirp.2019.04.074.
[29] M.A. De Pastre, A. Thompson, Y. Quinsat, J.A. Albajez García, N. Senin, R. Leach, Polymer powder bed fusion surface texture measurement, Meas. Sci. Technol. 31 (2020), https://doi.org/10.1088/1361-6501/ab63b1.
[30] R. Danzl, F. Helmli, S. Scherer, Focus variation - a robust technology for high resolution optical 3D surface metrology, Stroj. Vestnik/J. Mech. Eng. 57 (2011) 245–256, https://doi.org/10.5545/sv-jme.2010.175.
[31] T. Grimm, G. Wiora, G. Witt, Characterization of typical surface effects in additive manufacturing with confocal microscopy, Surf. Topogr. Metrol. Prop. 3 (2015), https://doi.org/10.1088/2051-672X/3/1/014001.
[32] Y. Shi, Z. Li, H. Sun, S. Huang, F. Zeng, Effect of the properties of the polymer materials on the quality of selective laser sintering parts, Proc. Inst. Mech. Eng. Part L J. Mater. Des. Appl. 218 (2004) 247–252, https://doi.org/10.1243/1464420041579454.
[33] A. Amado, M. Schmid, K. Wegener, Flowabillity of SLS Powders at Elevated Temperature, 2014, pp. 1–7, https://doi.org/10.3929/ETHZ-A-010057815.
[34] M. Pavan, M. Faes, D. Strobbe, B. Van Hooreweder, T. Craeghs, D. Moens, W. Dewulf, On the influence of inter-layer time and energy density on selected critical-to-quality properties of PA12 parts produced via laser sintering, Polym. Test. 61 (2017) 386–395, https://doi.org/10.1016/j.polymertesting.2017.05.027.
[35] I. Gibson, D. Shi, Material properties and fabrication parameters in selective laser sintering process, Rapid Prototyp. J. 3 (1997) 129–136, https://doi.org/10.1108/13552549710191836.
[36] M. Schmid, R. Kleijnen, M. Vetterli, K. Wegener, Influence of the origin of polyamide 12 powder on the laser sintering process and laser sintered parts, Appl. Sci. 7 (2017), https://doi.org/10.3390/app7050462.
[37] S. Berretta, O. Ghita, K.E. Evans, A. Anderson, C. Newman, Size, shape and flow of powders for use in selective laser sintering (SLS), in: High Value Manuf. Adv. Res. Virtual Rapid Prototyp. - Proc. 6th Int. Conf. Adv. Res. Rapid Prototyping, VR@P 2013, 2014, pp. 49–54, https://doi.org/10.1201/b15961-11.
[38] L. Verbelen, S. Dadbakhsh, M. Van Den Eynde, J.P. Kruth, B. Goderis, P. Van Puyvelde, Characterization of polyamide powders for determination of laser sintering processability, Eur. Polym. J. 75 (2016) 163–174, https://doi.org/10.1016/j.eurpolymj.2015.12.014.
[39] S. Dadbakhsh, L. Verbelen, O. Verkinderen, D. Strobbe, P. Van Puyvelde, J. P. Kruth, Effect of PA12 powder reuse on coalescence behaviour and microstructure of SLS parts, Eur. Polym. J. 92 (2017) 250–262, https://doi.org/10.1016/j.eurpolymj.2017.05.014.
[40] K. Dotchev, W. Yusoff, Recycling of polyamide 12 based powders in the laser sintering process, Rapid Prototyp. J. 15 (2009) 192–203, https://doi.org/10.1108/13552540910960299.
[41] D.T. Pham, K.D. Dotchev, W.A.Y. Yusoff, Deterioration of polyamide powder properties in the laser sintering process, Proc. Inst. Mech. Eng. Part C J. Mech. Eng. Sci. 222 (2008) 2163–2176, https://doi.org/10.1243/09544062JMES839.
[42] N.K. Mavoori, S. Vekatesh, M. Manzoor Hussain, Investigation on surface roughness of sintered PA2200 prototypes using Taguchi method, Rapid Prototyp. J. 25 (2019) 454–461, https://doi.org/10.1108/RPJ-10-2017-0201.
[43] P.B. Bacchewar, S.K. Singhal, P.M. Pandey, Statistical modelling and optimization of surface roughness in the selective laser sintering process, Proc. Inst. Mech. Eng. Part B J. Eng. Manuf. 221 (2007) 35–52, https://doi.org/10.1243/09544054JEM670.
[44] Z. Zhu, S. Lou, C. Majewski, Characterisation and correlation of areal surface texture with processing parameters and porosity of High Speed Sintered parts, Addit. Manuf. 36 (2020), https://doi.org/10.1016/j.addma.2020.101402.
[45] A. Triantaphyllou, C.L. Giusca, G.D. Macaulay, F. Roerig, M. Hoebel, R.K. Leach, B. Tomita, K.A. Milne, Surface texture measurement for additive manufacturing, Surf. Topogr. Metrol. Prop. 3 (2015), https://doi.org/10.1088/2051-672X/3/2/024002.
[46] N.K. Myshkin, M.I. Petrokovets, A.V. Kovalev, Tribology of polymers: adhesion, friction, wear, and mass-transfer, Tribol. Int. 38 (2005) 910–921, https://doi.org/10.1016/j.triboint.2005.07.016.
[47] A. Abdelbary, Sliding mechanics of polymers, in: Wear Polym. Compos., Elsevier, 2014, pp. 37–66, https://doi.org/10.1533/9781782421788.37.
[48] G. Guan, M. Hirsch, Z.H. Lu, D.T.D. Childs, S.J. Matcher, R. Goodridge, K. M. Groom, A.T. Clare, Evaluation of selective laser sintering processes by optical coherence tomography, Mater. Des. 88 (2015) 837–846, https://doi.org/10.1016/j.matdes.2015.09.084.